Fault diagnosis in wind turbines based on ANFIS and Takagi–Sugeno interval observers

Esvan-Jesús Pérez-Pérez [a,b], Francisco-Ronay López-Estrada [a,*], Vicenç Puig [b], Guillermo Valencia-Palomo [c], Ildeberto Santos-Ruiz [a]

[a] *Tecnológico Nacional de México, IT Tuxtla Gutiérrez, TURIX-Dynamics Diagnosis and Control Group, Carretera Panam. km 1080, CP 29050, Tuxtla Gutiérrez, Chiapas, Mexico*
[b] *Universitat Politècnica de Catalunya, Institut de Robòtica i Informàtica Industrial, CSIC-UPC. Parc Tecnològic de Barcelona. C Llorens i Artigas 4-6, 08028, Spain*
[c] *Tecnológico Nacional de México, IT Hermosillo, Av. Tecnológico y Periférico Poniente, S/N, 83170, Hermosillo, Mexico*

ARTICLE INFO

Keywords:
Wind turbine control
Fault detection
Adaptive Neuro-Fuzzy Inference System
Takagi–Sugeno models
Interval observers

ABSTRACT

Wind turbine power generation is becoming one of the most critical renewable energy sources. As wind power grows, there is a need for better monitoring and diagnostic strategies to maximize energy production and increase its security. In this paper, a fault diagnosis approach based on a data-driven technique, which represents the system behavior employing a Takagi–Sugeno (TS) model, is developed. An adaptive neuro-fuzzy inference system (ANFIS) method is used to obtain a set of polytopic-based linear representations and a set of membership functions to interpolate the linear models of the convex TS model. Then, considering the TS model, a fault diagnosis strategy based on convex state observers generate residuals to detect and isolate sensor faults. Unlike other methods, this proposal only needs to be trained with fault-free data. The proposed methodology is tested under different fault scenarios on a well-known wind turbine benchmark built upon fatigue, aerodynamics, structures, and turbulence (FAST). The results demonstrate the method's effectiveness in detecting and isolating different sensor faults.

1. Introduction

With the growing demand for energy and concern about environmental problems, sustainable solutions have attracted enormous attention, among which wind energy has demonstrated outstanding characteristics such as availability and low-cost (Arshad & O'Kelly, 2019). Wind turbines have complex and nonlinear dynamics and operate under stochastic wind disturbances, centrifugal, gravitational, and gyroscopic loads (Rommel et al., 2020). Relying on various rotating and non-rotating components and sensors, as well as working in harsh environments, makes them prone to severe faults and breakdowns, leading to poor reliability. To avoid unforeseen faults, maintenance schedules are planned, which not only increase cost but also reduce power generation due to the required downtime (Ntalampiras, 2021). These challenges have motivated numerous investigations in wind turbines, from nominal control to fault diagnosis, and fault-tolerant control.

Several fault diagnosis (FD) schemes have been proposed to increase safety, reliability and reduce maintenance costs. In general, architectures for FD employ sensor data for detecting, isolating, and identifying faults in components that can be used to implement fault-tolerant control and condition-based maintenance (Yu et al., 2021). Due to the lack of available data, many articles are based on synthetic data from a benchmark described in Odgaard et al. (2013). This benchmark represents a 5 MW wind turbine, which is commonly used to validate different FD approaches such as a model-based Kalman filter (Honarbari et al., 2021), an observer-based approach (Chouiref et al., 2017), a support vector machine method (Noshirvani et al., 2018), a multi-integral proportional observer (Fadali et al., 2019), adaptive observers (Li et al., 2020), a reduced-order sliding mode observer (Sedigh Ziyabari et al., 2021), among others. Most of well-established FD approaches are based on accurate mathematical models that can be affected by uncertainty and disturbances. However, obtaining an accurate wind turbine model is a difficult task in practice, which still limits the application of model-based approaches (Li et al., 2021). Recently, data-driven methods are currently receiving considerable attention (Simani et al., 2021). Unlike model-based approaches that require dynamic equations, data-driven methods rely on data from measured process variables.

* Corresponding author.
E-mail addresses: esvandejesus@gmail.com (E.-J. Pérez-Pérez), frlopez@ittg.edu.mx (F.-R. López-Estrada), vicenc.puig@upc.edu (V. Puig), gvalencia@hermosillo.tecnm.mx (G. Valencia-Palomo), Ildeberto.dr@tuxtla.tecnm.mx (I. Santos-Ruiz).

Robust FD strategies can also be grounded in data-driven solutions. For example, in Rezamand et al. (2019), principal component analysis (PCA) was used to detect gearbox faults. Diagnosis and classification schemes based on artificial neural networks (ANN) have also been implemented (Dybkowski & Klimkowski, 2019; Zare & Ayati, 2021). In Márquez-Vera et al. (2021), fault detection schemes based on fuzzy logic were proposed, a hybrid scheme for FD was reported in Wen and Xu (2021), where a ReliefF-PCA and deep neural networks (DNN) were combined. However, these methods require data under different fault conditions and sufficient data for training. Nevertheless, in practice, not all possible faults types are known or are not available; thus, it is difficult to access all the fault characteristics in a large and complex wind turbine system. For this reason, appropriate methods for the available measurement data in the systems are required.

This paper proposes an adaptive neuro-fuzzy inference system (ANFIS) to identify a set of analytical redundancy relations (ARRs) for the wind turbine obtained from structural analysis. As a result a set of convex Takagi–Sugeno (TS) models (López-Estrada et al., 2019) are obtained for the different ARRs. The modeling uncertainty of each TS model is also obtained and represented in parametric form. The training data are obtained from the measurable variables in a complete fault-free scenario. Using the TS model of each ARR, a set of convex interval observers is designed to detect and isolate faults. Different fault scenarios on a wind turbine benchmark are considered to illustrate the effectiveness of the method. Therefore, the main contributions of this paper are

- A hybrid strategy of ANFIS and convex TS interval observers for the fault diagnosis in wind turbines.
- The proposed ANFIS-TS hybrid scheme identifies a set of ARRs for the wind turbine obtained from the structural analysis. A set of convex TS models for the ARRs is obtained.
- Modeling uncertainty of each convex TS model is included and is represented parametrically. The training data is obtained from the available variables in fault-free conditions.
- Convex interval observers are designed using the convex TS model for each ARR for fault diagnosis using an LMI approach.
- To illustrate the method's effectiveness, different fault scenarios are considered in a wind turbine benchmark.

The remaining of this document is organized as follows: Section 2 presents the structural analysis for the considered wind turbine system that is used for deriving a set of ARRs. Section 3 describes the convex Takagi–Sugeno model obtained from each ARR using non-faulty data and ANFIS. Section 4 presents the fault diagnosis scheme based on interval observers. Finally, Section 5 presents the conclusions.

2. Structural analysis for wind turbine model

This work considers the wind turbine benchmark proposed in Odgaard et al. (2013). The benchmark replicates a three-bladed horizontal axis wind turbine that considers turbulent wind speed as the system input. Each subsystem is coupled through inputs and outputs that interact to structure a complex and realistic electromechanical system. The benchmark is based on an offshore horizontal variable speed wind turbine with a full converter coupling and a rated power of 5 MW built upon fatigue, aerodynamics, structures, and turbulence (FAST) aeroelastic simulator. This simulator was developed by the National Renewable Energy Laboratory (NREL) and was certified by Germanischer Lloyd in 2005, as announced by the NREL, which means that it can be used worldwide for turbine certification. Various FD schemes have been proposed for this wind turbine benchmark, being this reason why it is the most used to simulate and validate different schemes (Fadali et al., 2019).

The FD scheme of this work uses structural analysis, which describes the interactions between the signals and the wind turbine components.

Table 1
Components of wind turbine with respective ARRs and variables.

ARR	Related variables	Component
1	$P_g = \omega_g \tau_g$	Generator/converter
2	$\tau_{g,r} = \tau_g + \hat{\tau}_g$	Generator/converter
3	$\beta_{r,1} = \hat{\beta}_1 + \beta_1$	Pitch system
4	$\beta_{r,2} = \hat{\beta}_2 + \beta_2$	Pitch system
5	$\beta_{r,3} = \hat{\beta}_3 + \beta_3$	Pitch system
6	$(\hat{\omega}_r, \omega_r, \tau_r, \tau_g) = 0$	Drivetrain
7	$(\hat{\omega}_g, \omega_g, \tau_r, \tau_g) = 0$	Drivetrain
8	$\omega_r = \dot{\phi}_r$	Drivetrain
9	$(\Xi_e, \omega_{y,r}) = 0$	Yaw system
10	$M_{B,1} = \ddot{x}_x$	Tower
11	$M_{B,2} = \ddot{x}_x$	Tower
12	$M_{B,3} = \ddot{x}_x$	Tower

The dynamic model is interpreted as a set of constraints and a set of variables, which leads to a bipartite graph representing the system's structure. The structural analysis proposes a description of the nominal behavior of the system (fault-free) utilizing a description of each component and the connection they have among the known variables (measurements). Using this concept, it is possible to diagnose whether a violation of the nominal behavior has occurred.

In the case of a wind turbine, it is enough to know the relationships between variables and components. Fig. 1, shows the interaction between components and system variables; for each of these variables, there is an associated sensor. The components and measured variables are associated as follows. The wind speed v_w is the kinetic energy that drives the system. The rotor blades move due to the wind impulse and the pitch system regulates the angle of the blades β_l. The drivetrain connects a low-speed shaft to the rotor ω_r, the gears increase the rotation speed to the high-speed shaft ω_g and decrease the torque τ_g that drives the generator, coupled to a converter, to produce electrical power P_g. The tower contains the nacelle, which is deflected by loads and flexibility, causing the nacelle movement characterized by the acceleration in X and Y directions $\begin{bmatrix} \ddot{x}_X & \ddot{x}_Y \end{bmatrix}^T$. Additionally, there are complementary sensors in the system, an azimuth angle sensor ϕ_m is available for the low-speed shaft that connects the rotor to the drivetrain. A sensor for each of the three-blade root moment $M_{B,l}$ and a sensor to measure the yaw error Ξ_e. The controlled inputs of the system are the generator reference torque $\tau_{g,r}$, the reference angle of the blades β_r and yaw reference angular velocity $\omega_{y,r}$. The aerodynamic torque of the rotor τ_r is estimated from the wind speed v_w.

Consequently, there are enough sensors to measure the variables linking the components. Fig. 2 shows the structure graph of the components and measured variables. From the information in this graph, the ARRs can be generated. ARRs are available when matching components and measured variables (Blanke et al., 2006). Table 1 contains the components of the wind turbine and the ARRs that are generated from the relationships with the measured variables.

The purpose of the ARRs is to generate residuals for fault diagnosis. These residuals are used to check if the behavior of the system is within the nominal operating limits. Violation of the allowed limits is considered a fault. Residuals are computed as the difference between the measured and predicted behavior. The ARRs can be static, such as ARR1, ARR8 and ARR9 in Table 1, while the nine remaining ARRs are dynamic. The residual computation of the static ARRs is simple since they are derived from mathematical expressions. The dynamic ARRs are generated by comparing measured and observer-based estimation signals. The expression of each dynamic ARR model is calibrated in regressive form, as shown in Table 2.

ARRs in regressive form have the purpose of incorporating the dynamic behavior of the system. Each dynamic expression of ARR in regressive form from Table 2 is converted into an ANFIS model to structure a convex TS system and design the respective TS observer.

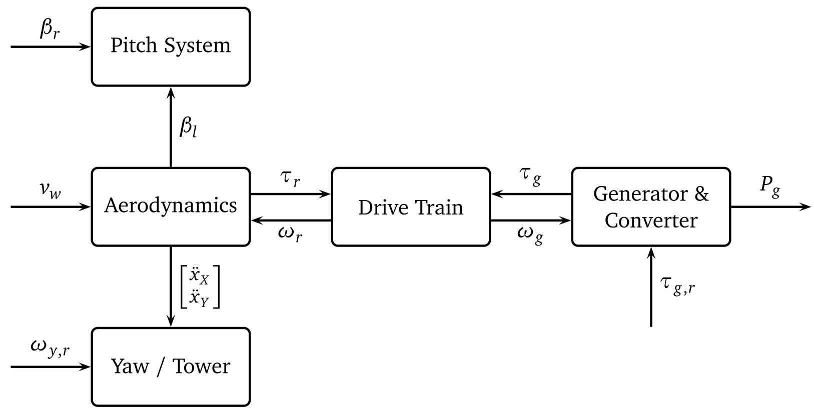

Fig. 1. Interaction of components and variables of the wind turbine model.

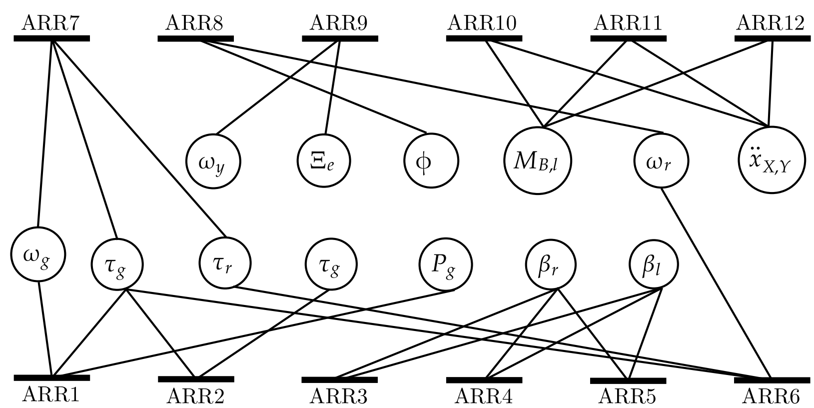

Fig. 2. Structure graph of the components and variables of the wind turbine.

Table 2
Expressions in regressive form for each dynamic ARR.

Variable	Regressive form
$\hat{\tau}_g(k)$	$\left(\tau_g(k), \tau_g(k-1), \tau_{gr}(k), \tau_{gr}(k-1)\right)$
$\hat{\beta}_1(k)$	$(\beta_1(k), \beta_1(k-1), \beta_1(k-2), \beta_r(k), \beta_r(k-1))$
$\hat{\beta}_2(k)$	$(\beta_2(k), \beta_2(k-1), \beta_2(k-2), \beta_r(k), \beta_r(k-1))$
$\hat{\beta}_3(k)$	$(\beta_3(k), \beta_3(k-1), \beta_3(k-2), \beta_r(k), \beta_r(k-1))$
$\hat{\omega}_r(k)$	$\left(\omega_r(k), \omega_r(k-1), \omega_r(k-2), \tau_g(k), \tau_r(k)\right)$
$\hat{\omega}_g(k)$	$\left(\omega_g(k), \omega_g(k-1), \omega_g(k-2), \tau_g(k), \tau_r(k)\right)$
$\hat{M}_{B,1}(k)$	$(M_{B,1}(k), M_{B,1}(k-1), \ddot{x}_x(k), \ddot{x}_x(k-1))$
$\hat{M}_{B,2}(k)$	$(M_{B,2}(k), M_{B,2}(k-1), \ddot{x}_x(k), \ddot{x}_x(k-1))$
$\hat{M}_{B,3}(k)$	$(M_{B,3}(k), M_{B,3}(k-1), \ddot{x}_x(k), \ddot{x}_x(k-1))$

3. Fault diagnosis based on ANFIS and convex Takagi–Sugeno interval observers

This section presents the proposed method for fault diagnosis based on ANFIS and convex TS interval observers. The scheme flow chart is presented in Fig. 3. The general idea is to obtain uncertain convex TS models for each of the dynamic ARRs using ANFIS. Subsequently, use the obtained convex TS models to design a bank of convex TS interval observers. Finally, use the observers designed for fault detection through the residuals generation and their evaluation with adaptive thresholds; and for fault isolation using a fault (incidence) matrix. These three stages are described next. The section ends with the considered fault scenarios.

3.1. Convex Takagi–Sugeno system from ANFIS

An ANFIS is considered to learn a particular structure from input–output data and approximate nonlinear systems behaviors (Alcala et al., 2020). In this work, an ANFIS is used to approximate each wind turbine subsystem's nonlinear behavior employing a set of fuzzy if-then rules and convex Takagi–Sugeno models. The objective is to obtain an approximated model for fault diagnosis, although the data sets for the learning stage are comprised of fault-free sensor data. The input data for the ANFIS are composed of each regressive expression of Table 2, which represents the wind turbine in nominal operating conditions. The training provides a set of consequent parameters and a set of premise parameters that define the membership functions (MF) of the convex TS models, producing nonlinear relationships between the different linear polynomials. The MFs used for this procedure are Generalized Bell-Shaped (GB) functions. GB functions have proven to obtain the best performance in nonlinear model approximation (Dorzhigulov & James, 2019).

Fig. 4 depicts the construction of the convex TS model $\hat{\omega}_g$ for approximating subsystem ω_g. The input dataset is comprised of the variables in the regression form of ω_g, presented in Table 2; namely, $\tau_g(k)$, $\tau_r(k)$, $\omega_g(k)$ and its delays $\omega_g(k-1)$ and $\omega_g(k-2)$. The ANFIS adjusts the premise and consequent parameters during the learning stage. Once the learning has finished, it proceeds to construct the convex TS representation for the $\hat{\omega}_g$ ARR.

The inputs to the ANFIS are weighted by means of the membership functions during the learning process until the neuro-fuzzy parameters are optimized. The ANFIS uses backpropagation and recursive least squares methods to adjust the consequent parameters during the learning stage. Once the learning has finished and the premise and

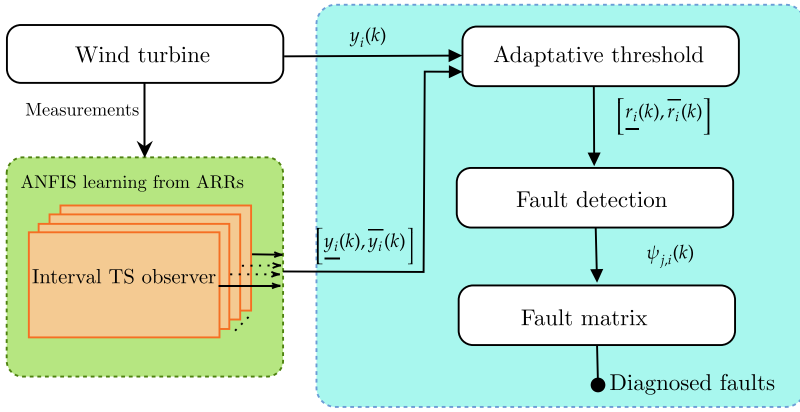

Fig. 3. Flow chart for the fault diagnosis based on ANFIS and convex Takagi–Sugeno interval observers.

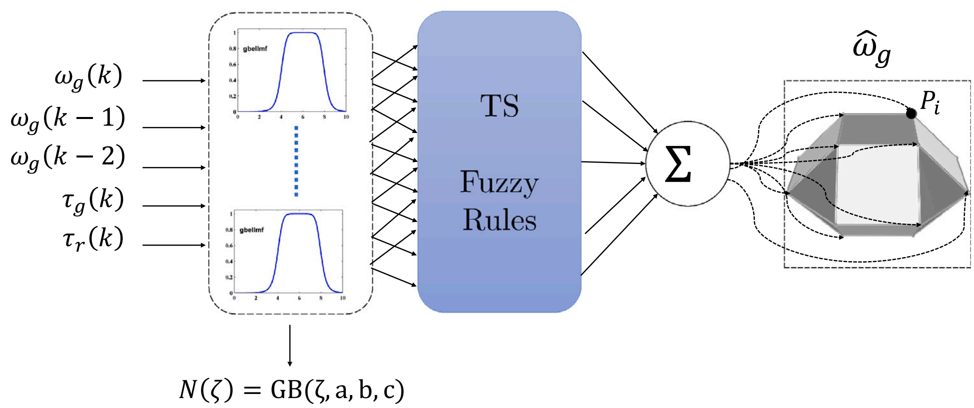

Fig. 4. Polytopic TS learning scheme for the subsystem case $\hat{\omega}_g$.

consequent parameters for each ANFIS have been calculated, it proceeds to construct the convex TS representation for each wind turbine subsystem. Therefore, for the polynomial representation, the case of the subsystem $\hat{\omega}_g$ will be used; it is formulated as:

$$P_i = p_{1i}\omega_g(k) + p_{2i}\omega_g(k-1) + p_{3i}\omega_g(k-2) + p_{4i}\tau_g(k) + p_{5i}\tau_r(k) + p_{6i},$$
$$\forall i = 1,\dots,N_v, \tag{1}$$

where P_i is a linear polynomial representation of a subsystem, $p_{ji}, \forall_j = 1,\dots,N_\zeta$ are the system parameters obtained from ANFIS; N_ζ represents the number of premise parameters as displayed in Fig. 4; and N_v represents the number of vertices. Terms in (1) can be rearranged as:

$$P_i = \begin{bmatrix} p_{1i} & p_{2i} & p_{3i} \\ p_{1i}^{I} & p_{2i}^{I} & p_{3i}^{I} \\ p_{1i}^{II} & p_{2i}^{II} & p_{3i}^{II} \end{bmatrix} x + \begin{bmatrix} p_{4i} & p_{5i} \\ p_{4i}^{I} & p_{5i}^{I} \\ p_{4i}^{II} & p_{5i}^{II} \end{bmatrix} u + \begin{bmatrix} p_{6i} \\ p_{6i}^{I} \\ p_{6i}^{II} \end{bmatrix}, \tag{2}$$

where $x = \begin{bmatrix} \omega_g(k) & \omega_g(k-1) & \omega_g(k-2) \end{bmatrix}^T$ is the state vector and $u = \begin{bmatrix} \tau_g & \tau_r \end{bmatrix}^T$ is the input vector. The polynomial structure is transformed to a discrete-time state-space representation as:

$$x(k+1) = A_i x(k) + B_i u(k) + h_i, \quad \forall i = 1,\dots,N_v, \tag{3}$$

where A_i, B_i and h_i are constant matrices structured from the consequent parameters of the polynomial structure. The membership function is constructed by considering the GB function, which is defined by three neuro-fuzzy parameters as follows:

$$\eta_m(\zeta_o) = \frac{1}{1 + \left|\frac{\zeta_o - c_{mo}}{a_{mo}}\right|^{2b_{mo}}}, \quad \forall m = 1,\dots,N_{MF}, \quad \forall o = 1,\dots,N_\zeta, \tag{4}$$

where a, b, c determines the width, slope, and center of the GB function, respectively; ζ represents the vector of ANFIS input variables (from now on, it will be referred to as premise parameter), N_{MF} represents the number of MF per premise parameter. For a common case where N_{MF} is two, then the normalized weights (η_{N_i}) are calculated as follows:

$$\mu_i(\zeta) = \prod_{j=1}^{N_\zeta} \xi_{ij}(\eta_0, \eta_1), \quad \forall i = 1,\dots,N_v, \tag{5}$$

where $\zeta_{ij}(\cdot)$ corresponds to any of the weighting functions that depend on each ith rule, such as the normalized weights are obtained as:

$$\mu_{N_i}(\zeta) = \frac{\mu_i(\zeta)}{\sum_{j=1}^{N_v} \mu_j(\zeta)}, \quad \forall i = 1,\dots,N_v. \tag{6}$$

Each premise parameter ζ_o is estimable and varies in a defined interval $\zeta_o \in \left[\underline{\zeta_o}, \overline{\zeta_o}\right] \in \mathbb{R}$. The polytopic TS model for each subsystem is obtained as:

$$x(k+1) = \sum_{i=1}^{N_v} \mu_{N_i}(\zeta(k))\Big(A_i x(k) + B_i u(k) + h_i\Big),$$
$$y(k) = Cx(k), \tag{7}$$

N_v is obtained by $N_v = \left(N_{MF}\right)^{N_\zeta} = 32$. It is important to mention that uncertainties are part of the model due to noise, model mismatches, and the method itself. Taking into account these issues, which are denoted by the ΔA_i matrices, system (7) is rewritten as:

$$x(k+1) = \sum_{i=1}^{N_v} \mu_{N_i}(\zeta(k))\Big((A_i + \Delta A_i)x(k) + B_i u(k) + h_i\Big),$$
$$y(k) = Cx(k), \tag{8}$$

The values of the uncertain matrices are proportional to the values of the parameters, which are adjusted by the minimum deviation to wrap the nominal values of the convex model. This uncertain representation will be used to apply a fault diagnosis method based on interval observers whose main advantage is to consider bounded initial conditions/parameters and generate adaptive residual thresholds that provides robustness to the fault diagnosis process. Nonetheless, in order to reduce the complexity, only uncertainties in A_i are considered. This assumption does not reduce the method applicability as discussed in Li et al. (2019), Martínez-García et al. (2020) and Xie et al. (2021). The fit is performed iteratively during ANFIS learning, where recursive least squares (RLS) is responsible for calculating the optimal values of the covariance matrix that will contain the uncertainty on the parameters. Furthermore, it is assumed that the uncertainties are bounded as follows:

$$\underline{\Delta A_i} \leq \Delta A_i \leq \overline{\Delta A_i}. \tag{9}$$

It is important to note that the uncertain model (8) is obtained by considering only fault-free data. Therefore, its structure is independent of the different types of faults that can affect the components of the wind turbine, which be discussed below by considering a fault diagnosis observer.

The fault diagnosis test is based on residual generation by checking whether the measurements are consistent with the system data or not. However, due to parametric uncertainty, an exact estimate of the state $x(k)$ cannot be obtained to compare the data directly. However, considering (8), an observer is designed that provides an interval estimate of $x(k)$, that is, some lower and upper estimates of $x(k)$, such that:

$$\underline{\hat{x}}(k) \leq x(k) \leq \overline{\hat{x}}(k). \tag{10}$$

Then, by considering this uncertain system, the following fault diagnosis observer is proposed.

3.2. Fault diagnosis based on interval observers

Generally, fault detection obtains residuals comparing the measured and estimated outputs. However, due to the uncertainties considered in System (8), which could corrupt the signals, it is essential to obtain residuals that are not affected by these uncertainties. Interval observers have proven to be efficient for uncertain systems because they can estimate states in upper and lower intervals of the variables to be estimated. The convex interval observer considered in this work has the following form:

$$\begin{aligned}
\underline{\hat{x}}(k+1) = \sum_{i=1}^{N_v} \mu_{N_i}(\zeta(k))\Big(&(A_i - \underline{L}_i C)\underline{\hat{x}}(k) + B_i u(k) + h_i + \underline{\Delta A_i}^{+}\underline{\hat{x}}^{+}(k) \\
&- \overline{\Delta A_i}^{+}\underline{\hat{x}}^{-}(k) - \underline{\Delta A_i}^{-}\underline{\hat{x}}^{+}(k) + \overline{\Delta A_i}^{-}\overline{\hat{x}}^{-}(k) + \underline{L}_i y(k)\Big), \\
\overline{\hat{x}}(k+1) = \sum_{i=1}^{N_v} \mu_{N_i}(\zeta(k))\Big(&(A_i - \overline{L}_i C)\overline{\hat{x}}(k) + B_i u(k) + h_i + \overline{\Delta A_i}^{+}\overline{\hat{x}}^{+}(k) \\
&- \underline{\Delta A_i}^{+}\overline{\hat{x}}^{-}(k) - \overline{\Delta A_i}^{-}\underline{\hat{x}}^{+}(k) + \underline{\Delta A_i}^{-}\underline{\hat{x}}^{-}(k) + \overline{L}_i y(k)\Big),
\end{aligned} \tag{11}$$

where $\underline{L}_i$ and $\overline{L}_i$ are the observer gain matrices to be computed. $\overline{\Delta A_i}^{+} = \max\left\{0, \overline{\hat{x}}\right\}$, $\overline{\Delta A_i}^{-} = \overline{\Delta A_i}^{+} - \overline{\Delta A_i}$, $\underline{\Delta A_i}^{+} = \max\left\{0, \underline{\hat{x}}\right\}$, $\underline{\Delta A_i}^{-} = \underline{\Delta A_i}^{+} - \underline{\Delta A_i}$, $\overline{\hat{x}}^{+} = \max\left\{0, \overline{\hat{x}}\right\}$, $\overline{\hat{x}}^{-} = \overline{\hat{x}}^{+} - \overline{\hat{x}}$, $\underline{\hat{x}}^{+} = \max\left\{0, \underline{\hat{x}}\right\}$, $\underline{\hat{x}}^{-} = \underline{\hat{x}}^{+} - \underline{\hat{x}}$. The upper and lower values of the estimated output are obtained as:

$$\underline{y}(k) = C^{+}\underline{\hat{x}}(k) - C^{-}\overline{\hat{x}}(k) \tag{12}$$

$$\overline{y}(k) = C^{+}\overline{\hat{x}}(k) - C^{-}\underline{\hat{x}}(k) \tag{13}$$

where $C^{+} = \max\{0, C\}$ and $C^{-} = C^{+} - C$, subject to the observer equations given by (11). The main problem is to compute the gain matrices of the interval observer (11), such as the estimated states converge asymptotically to (12) and (13) despite the uncertainties. Under the assumption that:

$$\underline{\hat{x}}(0) \leq x(0) \leq \overline{\hat{x}}(0). \tag{14}$$

The following sufficient conditions in the linear matrix inequalities (LMI) formulation are considered to solve this problem:

Theorem 3.1 (*Rotondo et al., 2016*). *Given an LMI region, defined as:*

$$\mathscr{D} = \left\{z \in : f_{\mathscr{D}}(z) < 0\right\}, \tag{15}$$

where the characteristic function $f_{\mathscr{D}(z)}$ is defined as:

$$f_{\mathscr{D}(z)} = \alpha + z\varphi + z^{*}\varphi^{T} = \left\{\alpha_{kl} + \varphi_{kl} z + \varphi_{lk} z^{*}\right\}_{k,l\in[1,m]}, \tag{16}$$

with $\alpha = \alpha^{T} \in \mathbb{R}^{mxm}$ and $\varphi \in \mathbb{R}^{mxm}$, if there exist a diagonal matrix $P \in \mathbb{R}^{2n_x x 2n_x}$, a symmetric matrix $Q = Q^{T} \in \mathbb{R}^{2n_x x 2n_x}$, block diagonal matrices $W_i \in \mathbb{R}^{2n_x x 2n_x}, i = 1, \ldots, N$, with the following structure:

$$W_i = \begin{pmatrix} \underline{W_i} \in \mathbb{R}^{n_x x n_x} & 0 \\ 0 & \overline{W_i} \in \mathbb{R}^{n_x x n_x} \end{pmatrix} \tag{17}$$

and constants $\varepsilon_1 > 0$, $\varepsilon_2 > 0$, $\gamma > 0$ such that:

$$P > 0 \tag{18}$$

$$Q > 0 \tag{19}$$

and, for i = 1,...,N:

$$\begin{pmatrix} \frac{P}{1+\varepsilon_1} & PD_i - W_i\gamma & \frac{P}{1+\varepsilon_1} \\ (PD_i - W_i\gamma)^{T} & P - Q - \gamma\eta^{2} I_{2n_x} & 0 \\ \frac{P}{1+\varepsilon_1} & 0 & \gamma I_{2n_x} - \varepsilon P \end{pmatrix} \geq 0 \tag{20}$$

$$P\begin{bmatrix} A_i & 0 \\ 0 & A_i \end{bmatrix} - W_i\gamma \geq 0 \tag{21}$$

$$\begin{cases} \alpha_{kl} P + \varphi_{kl}\left(\begin{pmatrix} A_i^{T} & 0 \\ 0 & A_i^{T} \end{pmatrix} P - \gamma^{T} W_i^{T}\right) \\ +\varphi_{kl}\left(P\begin{pmatrix} A_i & 0 \\ 0 & A_i \end{pmatrix} - W_i\gamma\right)_{k,l\in[1,m]} \quad < 0 \end{cases} \tag{22}$$

with:

$$D_i = \begin{pmatrix} A_i + \underline{\Delta A_i}^{+} & 0 \\ 0 & A_i + \overline{\Delta A_i}^{+} \end{pmatrix} \tag{23}$$

$$\gamma = \begin{pmatrix} C & 0 \\ 0 & C \end{pmatrix} \tag{24}$$

$$\eta = 2\max_{i=1,\ldots,N}\left(\|\underline{\Delta A_i}^{+} - \overline{\Delta A_i}^{+}\|_2 + \|\underline{\Delta A_i}^{-}\|_2 + \|\overline{\Delta A_i}^{-}\|_2\right) \tag{25}$$

$$\varepsilon = 1 + \varepsilon_2 + (1+\varepsilon_1)^{-1} \tag{26}$$

then, the TS interval observer (11) with gains calculated as:

$$\underline{L} = P^{-1}\underline{W}_i \tag{27}$$

$$\overline{L} = P^{-1}\overline{W}_i \tag{28}$$

ensure the estimation of the interval x(k) given by (10), provided that (11) and *(14) are fulfilled.*

The overall system of LMIs (18),(19),(20),(21) and (22) can be solved efficiently using available solvers, as YALMIP toolbox. The proof of the theorem can be consulted in Rotondo et al. (2016).

3.3. Fault diagnosis based on residual generation

By considering the estimated outputs (12)–(13), the following residuals can be obtained as:

$$\underline{r}(k) = y(k) - \overline{y}(k); \tag{29}$$

$$\overline{r}(k) = y(k) - \underline{y}(k); \tag{30}$$

where $r(k) \in \mathbb{R}^{N_y}$ is the residual. In the ideal case, $r(k) \approx 0$ if there are no faults present. However, it may be non-zero in a fault-free scenario due to measurement noise, modeling errors, among others.

A robust passive approach based on an adaptive threshold can be used (Puig et al., 2008). Thus, using this passive approach, the impact of the parameter uncertainties on the residual $r(k)$ associated with each output of the system $y(k)$ is bounded by an interval that will include the zero value in the absence of faults. Therefore, a fault detection test can be formulated as:

$$y(k) \in \left[\underline{y}(k), \overline{y}(k)\right] \tag{31}$$

where $y(k)$ is the sensor output, and $\underline{y}(k)$ and $\overline{y}(k)$ are the limits of the predicted output given by (12) and (13).

The residuals are derived from the ARRs described in Section 2, the respective observers will be designed for the dynamic residuals:

$$r_1(k) = P_g(k) - \hat{P}_g(k)(\omega_g(k), \tau_g(k)), \tag{32}$$

$$r_2(k) = \tau_g(k) - \hat{\tau}_g(k), \tag{33}$$

$$r_{l+2}(k) = \beta_l(k) - \hat{\beta}_l(k), \tag{34}$$

$$r_6(k) = \omega_r(k) - \hat{\omega}_r(k), \tag{35}$$

$$r_7(k) = \omega_g(k) - \hat{\omega}_g(k), \tag{36}$$

$$r_8(k) = \phi_r(k) - \hat{\phi}_r(k)(\phi_r(k), \omega_r(k)), \tag{37}$$

$$r_9(k) = \Xi_e(k) - \hat{\Xi}_e(k)(\Xi_e(k), \omega_{y,r}(k)), \tag{38}$$

$$r_{9+l}(k) = M_{B,l}(k) - \hat{M}_{B,l}(k), \quad l = 1, 2, 3. \tag{39}$$

The equations mentioned above search to generate residuals sensitive only to one fault. However, from the obtained ARRs, it is clear that some faults cannot be isolated because the same fault activates different residuals. In this scenario, the method only guarantees the detection but not the isolation.

In a fault scenario, the residuals are activated when exceeding the limits of the interval. If the interval limits are well-defined, then all false alarms can be avoided because the ARR guarantee the separability of the effect of each fault on the residuals. These residuals are stored in a fault incidence matrix, whose elements are constructed by considering the following logic:

$$\psi_{j,i}(k) = \begin{cases} 0 & \text{if} \quad r_i(k) \in \left[\underline{r_i}(k), \overline{r_i}(k)\right] \\ 1 & \text{if} \quad r_i(k) \notin \left[\underline{r_i}(k), \overline{r_i}(k)\right] \end{cases}, \forall j \in [1, \dots, N_f],$$
$$\forall i \in [1, \dots, N_y] \tag{40}$$

where N_f is the number of faults. Fault isolation is done by evaluating the incidence matrix and the knowledge of the binary relationship between the residuals.

3.4. Fault scenarios

The FAST wind turbine benchmark covers different types of possible faults, as listed in Table 3. These faults have different degrees of severity; some are very serious and should result in a quick and safe shutdown; other faults are less severe and can cause a performance degradation. Different numerical simulations are carried out for the diagnostic scheme based on Table 3. Each fault scenario is related to different types of faults that can occur in a real environment (sensors, actuators or components). The results obtained are described in the next section.

4. Results

This section presents the results of the fault diagnosis obtained from numerical simulations carried out in the benchmark described in Odgaard et al. (2013). The wind speed used for the simulations was 17 m/s on average with the profile shown in Fig. 5. The simulations were carried out for a time interval of 630 s with a sampling frequency of 80 Hz, counting 50 401 samples per variable in the data vectors.

Table 3
Faults simulated in the benchmark.

Fault Class	Description	Type
Fault 1	Blade root bending moment sensor	Scaling
Fault 2	Accelerometer	Offset
Fault 3	Generator speed sensor	Scaling
Fault 4	Pitch angle sensor	Stuck
Fault 5	Generator power sensor	Scaling
Fault 6	Low speed shaft position encoder	Bit error
Fault 7	Pitch actuator	Abrupt
Fault 8	Pitch actuator	Slow
Fault 9	Torque offset	Offset
Fault 10	Yaw drive	Stuck drive

The mechanical and electrical parameters predefined in the benchmark were not changed, since the characteristics of the wind turbine model meet the requirements to perform FD tests in a realistic environment.

Fault-free simulations were performed to form the data sets for ANFIS training. The data sets were divided into 70% for training, 15% for validation, and 15% for testing. The number of fuzzy rules (FR) is related to the number of premise parameters of each ARR subsystem as $\mathrm{FR} = 2^{N_\zeta}$. For the case of $\hat{\omega}_g$, $\hat{\omega}_r$ and $\hat{\beta}_l$, 32 FRs were obtained; for $\hat{\tau}_g$ and $\hat{P}_g$, 16 FRs were obtained. Therefore, the number of local models was the same as FR for the TS representation. Due to the space limitation, the model is not presented here, but for $\hat{\beta}_l$, the corresponding model is:

$$x(k+1) = \sum_{i=1}^{N_v} \mu_{N_i}(\zeta(k))\Big((A_i + \Delta A_i)x(k) + B_i u(k) + h_i\Big),$$
$$y(k) = Cx(k), \tag{41}$$

where $x(k) = \left[\beta_l(k),\ \beta_l(k-1),\ \beta_l(k-2)\right]^T$ is the state vector and $u(k) = \left[\beta_r(k),\ \beta_r(k-1)\right]^T$ is the input vector. Then, by solving the LMIs (18)–(22) of Theorem 3.1, the following P matrix is obtained:

$$P = \begin{bmatrix} 0.5587 & 0.0759 & 0.0016 \\ 0.0853 & 0.02285 & 0.1763 \\ 0.0016 & 0.1763 & 0.7715 \end{bmatrix}; \tag{42}$$

where P is positive definite, valid for the set of matrices L_1 of system (41) and satisfies the stability and observability criteria. Due to the space limitation, the gain matrices are not displayed here but they can be easily calculated with Eqs. (27) and (28).

In Fig. 6, the result of the blade pitch angle interval observer is displayed, where the observer envelops the nominal signal of the β_l measurement.

In order to verify the performance of the proposed fault diagnosis method, the entire sequence of ten faults presented in Table 3 is applied. Faults were detected at the time of occurrence, established according to the detection and isolation requirements of the benchmark given in Odgaard et al. (2013). Table 4 display the incidence matrix constructed according to (40). Fault detection and isolation can be done easily by evaluating this matrix. For example, let us consider the fault on the torque sensor corresponding to fault 9 from $t = 495$ s to $t = 520$ s whose corresponding residuals are displayed in Fig. 7. As observed, the activated residuals are r_1, r_2, r_6, and r_7, which is congruent with the information displayed of the incidence matrix. Then, the fault isolation can be done by evaluating this particular signature with binary logic. A similar analysis can be done for the rest of the faults. Although the plots in Figs. 6 and 7 correspond only to the wind profile shown in Fig. 5, other tests with different wind profiles did not show significant variations in fault detectability/isolability.

Note that for faults 4, 7 and 8 the same residuals are activated, which means that these faults can be detected, but cannot be isolated. From the physical point of view, this situation occurs because they correspond to the same component of the pitch system. Since the proposed scheme is based on the ARRs, this issue represents an area of opportunity to explore other data-driven fault diagnosis schemes that could deal with these faults.

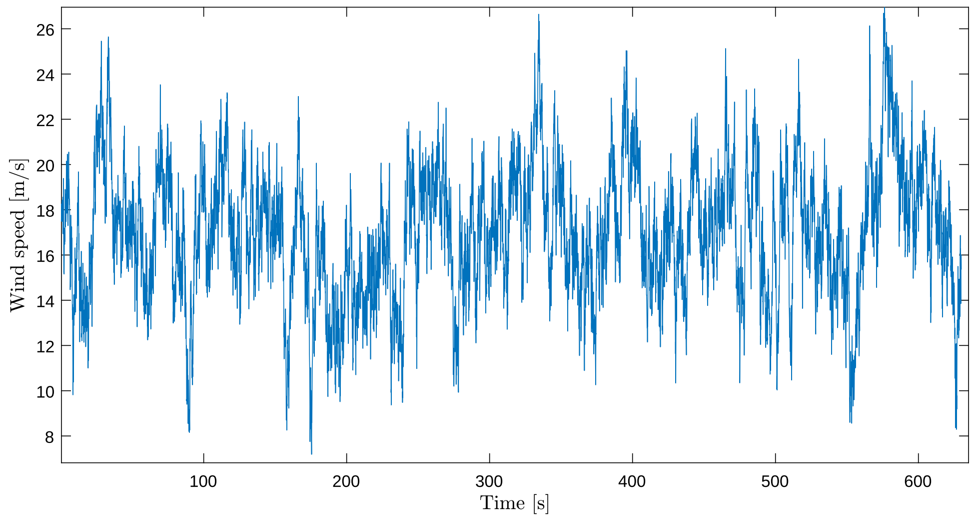

Fig. 5. Wind speed profile at hub height for simulation tests.

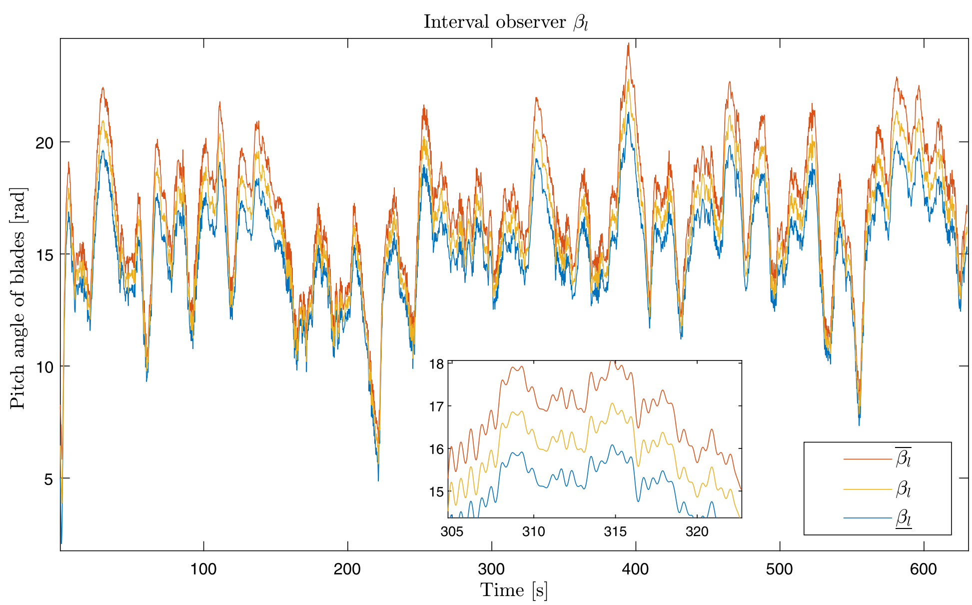

Fig. 6. Interval observer $\underline{\beta}_l$ and $\overline{\beta}_l$ of β_l.

Table 4
Incidence matrix for the set of fault scenarios considered in the benchmark.

Fault	r_1	r_2	r_3	r_4	r_5	r_6	r_7	r_8	r_9	r_{10}	r_{11}	r_{12}
1	0	0	0	0	0	0	0	0	0	1	1	1
2	0	0	0	0	0	0	0	0	0	1	1	1
3	1	0	0	0	0	0	1	0	0	0	0	0
4	0	0	1	1	1	0	0	0	0	0	0	0
5	1	0	0	0	0	0	0	0	0	0	0	0
6	0	0	0	0	0	0	0	1	0	0	0	0
7	0	0	1	1	1	0	0	0	0	0	0	0
8	0	0	1	1	1	0	0	0	0	0	0	0
9	1	1	0	0	0	1	1	0	0	0	0	0
10	0	0	0	0	0	0	0	0	1	0	0	0

To obtain a perspective of the effectiveness of the proposed method, it is compared with different FD schemes. Table 5 compares the reported detection time for different methods, taking as a reference the detection time requirements reported in Odgaard et al. (2013). The detection times (T_D) are in terms of the sampling time (T_s) which is 0.0125 s in this case. The first column is related to the fault number, and the second column displays the required detection time. The rest of the columns display different detection methods, including this paper's proposal. The results reported in the literature of four relevant methods are considered. A fusion classifier approach (CFA), reported in Pashazadeh et al. (2018) where a combination of three classifiers is used for fault detection: multilayer perceptron (MPL), k-nearest neighbor (KNN), and decision tree. Some of the faults can be detected within the time requirements, however, this method does not consider (NC) faults 1 and 7. A support vector machine and Kalman observer (SVMKO) used to isolate faults in different components proposed by Sheibat-Othman et al. (2013). This proposal marks NC three faults and only a few are within the requirements. A scheme combining support vector machine and residual (SVMR) techniques for FD of wind turbine faults proposed by Zeng et al. (2013). The results of this combined method meet the FD time requirements, but cannot detect fault 1. Interval observers based on ARRs (IOBA) presented by Sanchez et al. (2015) which is a model-based method and improves the previous FD results with respect to the number of faults that can be detected, but it strongly depends on the model and the calibration in its methodology. Finally, the approach presented in this work is shown in Table 5 as ANFIS-TS where its

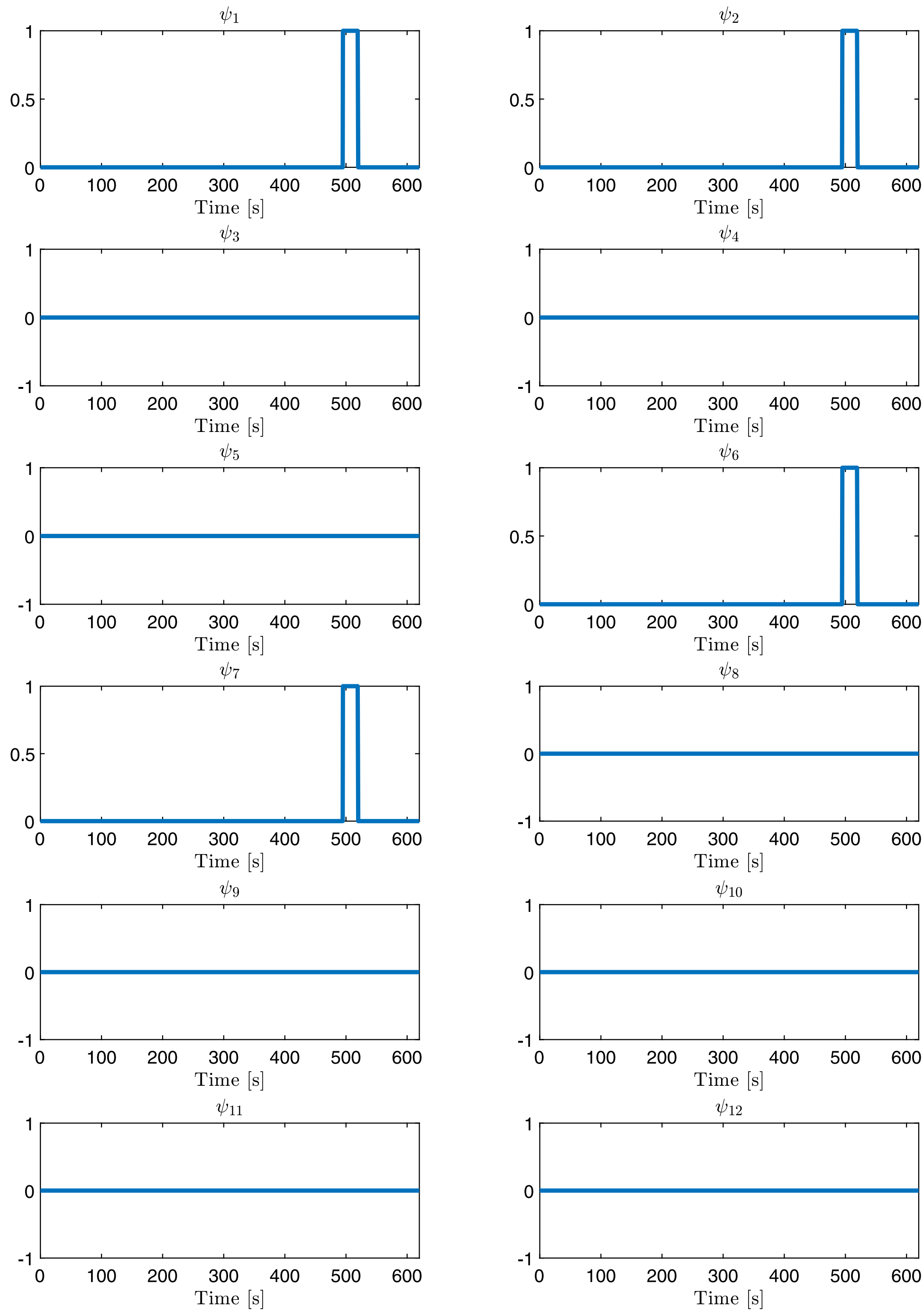

Fig. 7. Observed fault 9 signature in drive-train sensor.

effectiveness can be observed, being able to detect all faults in the required time.

With respect the FD times, the SVRM method can detect faults 2, 3, 7 and 8 slightly faster than the method proposed in this paper. It is important to mention that although SVRM can detect these faults faster; compared to the required time for detection, the difference with ANFIS-TS is minimal. While ANFIS-TS is superior for faults 4,6,9 and 10, where the improvement in detection time is more significant when the required time for detection is taken into account, particularly for faults 4 and 10. In addition, ANFIS-TS can detect fault 1, which SVRM cannot. The rest of the methods are clearly slower than ANFIS-TS. Thus, it can be concluded that ANFIS-TS is effective in FD, complying with the detection times and improving most of the FD times, demonstrating that when using the data-based methods and combining them with observers, the results are improved.

This work followed the standard way of adding the uncertainty by using the measured data covariance. Nevertheless, a better form of adding this uncertainty could be by considering them as part of the fuzzy identification of the ANFIS. On the other hand, the selected interval limits affect the fault diagnosis observer. To improve the method, techniques based on set membership can be implemented to propagate the uncertainties through zonotopic interval observers. Finally, faults 4, 7, and 8 can be detected but not isolated because of the construction of the residuals, which are based on the ARR. However, it is possible to implement an additional residual evaluation based on an ANN that could discern between the slight differences of the residuals and thus

Table 5
Comparison of results of different FD schemes.

Fault	T_D required	T_D obtained				
		ANFIS-TS	CFA	SVMKO	SVMR	IOBA
1	<10 T_s	2 T_s	NC	NC	NC	3 T_s
2	<10 T_s	7 T_s	17 T_s	3 T_s	6 T_s	18 T_s
3	<10 T_s	2 T_s	4 T_s	22 T_s	1 T_s	3 T_s
4	<10 T_s	2 T_s	7 T_s	44 T_s	6 T_s	3 T_s
5	<10 T_s	2 T_s	4 T_s	11 T_s	2 T_s	3 T_s
6	<10 T_s	4 T_s	13 T_s	34 T_s	6 T_s	6 T_s
7	<8 T_s	5 T_s	NC	NC	2 T_s	375 T_s
8	<100 T_s	9 T_s	11 T_s	12 T_s	2 T_s	33 T_s
9	<3 T_s	2 T_s	18 T_s	35 T_s	3 T_s	3 T_s
10	<50 T_s	3 T_s	32 T_s	NC	36 T_s	3 T_s

isolate the faults that are not possible with the method proposed in this article (see Puig & Blesa, 2013 where the residual order of activation is used for improving isolability).

5. Conclusions

In this work, a fault detection scheme for a wind turbine based on Takagi–Sugeno interval observers was proposed considering parametric uncertainty. Unlike other FD works, TS models are structured based on the measurements available in the system. The proposed method generates confidence intervals that represent the lack of knowledge due to modeling errors. It is verified that the fault-free measurements are within the intervals, avoiding false alarms.

Structural analysis of the wind turbine was carried out to obtain a bipartite graph that relates a set of components and a set of measured variables. Consequently, the ARRs that structured convex Takagi–Sugeno (TS) models were obtained with an approach based on neuro-fuzzy learning to identify the wind turbine dynamics. To get the convex TS representation with modeling uncertainty, the ANFIS were used, which were trained with fault-free data.

The Takagi–Sugeno observers were designed with fuzzy learning from inputs and outputs measurements. The fault diagnosis was addressed by a bank of interval TS observers with adaptable thresholds.

A convex TS system was obtained in the proposed methodology that considers the parametric uncertainty using only measurements and system data. Therefore, observers can be designed, and the LMIs improved. There is an exploit framework to implement methods without using the equations of the dynamic system. When no model faithfully represents a real system, considering the uncertainty bands represents a detection advantage in faults that are not modeled.

As future work, robust fault diagnostic schemes will be implemented, where the uncertainty propagates in the parameters, adding noise at the outputs. Another avenue that will be explored is the implementation of observers based on zonotopes.

CRediT authorship contribution statement

Esvan-Jesús Pérez-Pérez: Investigation, Software, Writing – original draft. **Francisco-Ronay López-Estrada:** Conceptualization, Methodology, Supervision, Writing – original draft, Project administration, Funding acquisition. **Vicenç Puig:** Conceptualization, Resources, Supervision, Writing – review & editing. **Guillermo Valencia-Palomo:** Formal analysis, Validation, Writing – review & editing. **Ildeberto Santos-Ruiz:** Validation, Data curation, Writing – review & editing.

Declaration of competing interest

The authors declare the following financial interests/personal relationships which may be considered as potential competing interests: Francisco-Ronay Lopez-Estrada reports financial support was provided by Tecnológico Nacional de México. Francisco-Ronay Lopez-Estrada reports financial support was provided by National Council on Science and Technology.

Acknowledgments

This research has been supported by the Consejo Nacional de Ciencia *y* Tecnología (CONACyT), Mexico under the grant *Becas Nacionales* and by Tecnológico Nacional de México under the program *Proyectos de Investigación Científica y Desarrollo Tecnológico e Innovación 2022*.

References

Alcala, E., Sename, O., Puig, V., & Quevedo, J. (2020). TS-MPC for autonomous vehicle using a learning approach. *IFAC-PapersOnLine*, *53*(2), 15110–15115.
Arshad, M., & O'Kelly, B. (2019). Global status of wind power generation: theory, practice, and challenges. *International Journal of Green Energy*, *16*(14), 1073–1090.
Blanke, M., Kinnaert, M., Lunze, J., Staroswiecki, M., & Schröder, J. (2006). *Vol. 2, Diagnosis and fault-tolerant control*. Springer.
Chouiref, H., Boussaid, B., Abdelkrim, M. N., Puig, V., & Aubrun, C. (2017). An LPV modelling and fault diagnosis in wind turbine benchmark system. *International Journal of Modelling, Identification and Control*, *27*(4), 243–255.
Dorzhigulov, A., & James, A. P. (2019). Generalized bell-shaped membership function generation circuit for memristive neural networks. In *2019 IEEE international symposium on circuits and systems (ISCAS)* (pp. 1–5). IEEE.
Dybkowski, M., & Klimkowski, K. (2019). Artificial neural network application for current sensors fault detection in the vector controlled induction motor drive. *Sensors*, *19*(3), 571.
Fadali, Y., Lahmadi, K., & Boumhidi, I. (2019). Fault detection and isolation for wind turbine system based on proportional multi-integral observer (PMIO). *International Journal of Automation and Smart Technology*, *9*(3), 121–137.
Honarbari, A., Najafi-Shad, S., Saffari Pour, M., Ajarostaghi, S. S. M., & Hassannia, A. (2021). MPPT improvement for PMSG-based wind turbines using extended Kalman filter and fuzzy control system. *Energies*, *14*(22), 7503.
Li, L.-L., Liu, Z.-F., Tseng, M.-L., Jantarakolica, K., & Lim, M. K. (2021). Using enhanced crow search algorithm optimization-extreme learning machine model to forecast short-term wind power. *Expert Systems with Applications*, *184*, Article 115579.
Li, C., Teng, J., Yang, T., & Feng, Y. (2020). Adaptive observer based fault detection and isolation for wind turbines. In *2020 Chinese automation congress (CAC)* (pp. 481–486). IEEE.
Li, J., Wang, Z., Zhang, W., Raissi, T., & Shen, Y. (2019). Interval observer design for continuous-time linear parameter-varying systems. *Systems & Control Letters*, *134*, Article 104541.
López-Estrada, F.-R., Rotondo, D., & Valencia-Palomo, G. (2019). A review of convex approaches for control, observation and safety of linear parameter varying and Takagi-Sugeno systems. *Processes*, *7*(11), 814.
Márquez-Vera, M., Ramos-Velasco, L., López-Ortega, O., Zúñiga-Peña, N., Ramos-Fernández, J., & Ortega-Mendoza, R. (2021). Inverse fuzzy fault model for fault detection and isolation with least angle regression for variable selection. *Computers & Industrial Engineering*, *159*, Article 107499.
Martínez-García, C., Puig, V., Astorga-Zaragoza, C.-M., Madrigal-Espinosa, G., & Reyes-Reyes, J. (2020). Estimation of actuator and system faults via an unknown input interval observer for Takagi-Sugeno systems. *Processes*, *8*(1), 61.
Noshirvani, G., Askari, J., & Fekih, A. (2018). A robust fault detection and isolation filter for the pitch system of a variable speed wind turbine. *International Transactions on Electrical Energy Systems*, *28*(11), Article e2625.
Ntalampiras, S. (2021). One-shot learning for acoustic diagnosis of industrial machines. *Expert Systems with Applications*, *178*, Article 114984.
Odgaard, P. F., Stoustrup, J., & Kinnaert, M. (2013). Fault-tolerant control of wind turbines: A benchmark model. *IEEE Transactions on Control Systems Technology*, *21*(4), 1168–1182.
Pashazadeh, V., Salmasi, F. R., & Araabi, B. N. (2018). Data driven sensor and actuator fault detection and isolation in wind turbine using classifier fusion. *Renewable Energy*, *116*, 99–106.
Puig, V., & Blesa, J. (2013). Limnimeter and rain gauge FDI in sewer networks using an interval parity equations based detection approach and an enhanced isolation scheme. *Control Engineering Practice*, *21*(2), 146–170.
Puig, V., Quevedo, J., Escobet, T., Nejjari, F., & de las Heras, S. (2008). Passive robust fault detection of dynamic processes using interval models. *IEEE Transactions on Control Systems Technology*, *16*(5), 1083–1089.
Rezamand, M., Kordestani, M., Carriveau, R., Ting, D. S., & Saif, M. (2019). A new hybrid fault detection method for wind turbine blades using recursive PCA and wavelet-based PDF. *IEEE Sensors Journal*.

Rommel, D., Di Maio, D., & Tinga, T. (2020). Calculating wind turbine component loads for improved life prediction. *Renewable Energy*, *146*, 223–241.

Rotondo, D., Fernandez-Canti, R. M., Tornil-Sin, S., Blesa, J., & Puig, V. (2016). Robust fault diagnosis of proton exchange membrane fuel cells using a Takagi-Sugeno interval observer approach. *International Journal of Hydrocarbon Engineering*, *41*(4), 2875–2886.

Sanchez, H., Escobet, T., Puig, V., & Odgaard, P. F. (2015). Fault diagnosis of an advanced wind turbine benchmark using interval-based ARRs and observers. *IEEE Transactions on Industrial Electronics*, *62*(6), 3783–3793.

Sedigh Ziyabari, S. H., Aliyari Shoorehdeli, M., & Karimirad, M. (2021). Robust fault estimation of a blade pitch and drivetrain system in wind turbine model. *Journal of Vibration and Control*, *27*(3–4), 277–294.

Sheibat-Othman, N., Othman, S., Benlahrache, M., & Odgaard, P. F. (2013). Fault detection and isolation in wind turbines using support vector machines and observers. In *2013 American control conference* (pp. 4459–4464). IEEE.

Simani, S., Farsoni, S., & Castaldi, P. (2021). Application of data–driven fault diagnosis design techniques to a wind turbine test–rig. In *Intelligent computing* (pp. 23–38). Springer.

Wen, X., & Xu, Z. (2021). Wind turbine fault diagnosis based on reliefF-PCA and DNN. *Expert Systems with Applications*, *178*, Article 115016.

Xie, Q., Ma, L., Fu, Q., Fan, Y., Chen, Z., & Wang, X. (2021). Interval observer design for a class of nonlinear time-varying systems with application in fault detection. In *2021 China automation congress (CAC)* (pp. 5742–5747). IEEE.

Yu, W., Lu, Y., & Wang, J. (2021). Application of small sample virtual expansion and spherical mapping model in wind turbine fault diagnosis. *Expert Systems with Applications*, *183*, Article 115397.

Zare, S., & Ayati, M. (2021). Simultaneous fault diagnosis of wind turbine using multichannel convolutional neural networks. *ISA Transactions*, *108*, 230–239.

Zeng, J., Lu, D., Zhao, Y., Zhang, Z., Qiao, W., & Gong, X. (2013). Wind turbine fault detection and isolation using support vector machine and a residual-based method. In *2013 American control conference* (pp. 3661–3666). IEEE.